View metadata, citation and similar papers at core.ac.uk

brought to you by CORE

provided by IntechOpen

We are IntechOpen, the world's leading publisher of Open Access books Built by scientists, for scientists

4,800
Open access books available

122,000
International authors and editors

135M
Downloads

Our authors are among the

154
Countries delivered to

TOP 1%
most cited scientists

12.2%
Contributors from top 500 universities

CLARIVATE ANALYTICS BOOK CITATION INDEX INDEXED

WEB OF SCIENCE™

Selection of our books indexed in the Book Citation Index in Web of Science™ Core Collection (BKCI)

Interested in publishing with us?
Contact book.department@intechopen.com

Numbers displayed above are based on latest data collected.
For more information visit www.intechopen.com

Chapter 5

Synthesis, Superhydrophobicity, Enhanced Photoluminescence and Gas Sensing Properties of ZnO Nanowires

M.G. Gong, Y.Z. Long, X.L. Xu, H.D. Zhang and B. Sun

Additional information is available at the end of the chapter

http://dx.doi.org/10.5772/52586

1. Introduction

The past decades have witnessed major worldwide interested in the fabrication of nanodevices based on quasi one-dimensional (1D) semiconducting nanostructures (Xu and Wang, 2011; Long *et al.*, 2011; Long *et al.*, 2012). ZnO, an important II-VI group semiconductor with many excellent properties (Xu and Wang, 2011), has been suggested for a diverse range of applications, including optoelectronics (Ko *et al.*, 2011; Wang *et al.*, 2004), ultraviolet laser devices (Liu *et al.*, 2011), gas sensors (Wang *et al.*, 2011; Ra *et al.*, 2008; Wang *et al.*, 2006) and transparent electrodes (Kusinski *et al.*, 2010; Goris *et al.*, 2009), etc. 1D ZnO nanorods, nanowires and nanofibers have been synthesized by a range of techniques, such as top-down approaches by etching (Wu *et al.*, 2004), and wet chemical methods (Vayssieres *et al.*, 2001; Gong *et al.*, 2009), metal-organic chemical vapor deposition (MOCVD) (Yang *et al.*, 2004; Pfüller *et al.*, 2011; Lee *et al.*, 2004), physical vapor deposition (Huang *et al.*, 2001; Jeong and Lee, 2010; Wang *et al.*, 2005; Hsu *et al.*, 2005), molecular beam epitaxy (MBE) (Heo *et al.*, 2002), pulsed laser deposition (Shen *et al.*, 2010; Cao *et al.*, 2007), sputtering (Chiou *et al.*, 2003), flux (Kong and Li, 2003), electrospinning (Sen *et al.*, 2011; Wu *et al.*, 2008; Lin *et al.*, 2007; Sui *et al.*, 2005) methods, etc.

Among those techniques, MOCVD and MBE can yield high quality ZnO nanowires arrays, but usually suffer from low product yield, poor deposition uniformity, and limited choices of substrate. Especially, the fabrication cost is usually very high, so they have been less widely used. The physical vapor deposition and flux methods usually require high temperature, which are less likely to be able to integrate with flexible organic substrates for future

INTECH
open science | open minds

© 2012 Gong et al.; licensee InTech. This is an open access article distributed under the terms of the Creative Commons Attribution License (http://creativecommons.org/licenses/by/3.0), which permits unrestricted use, distribution, and reproduction in any medium, provided the original work is properly cited.

foldable and portable electronics, and can easily incorporate catalysts or other impurities into the ZnO nanowires. Top-down, pulsed deposition and sputtering approaches have less reproducibility and controllability compared with other techniques. Electrospinning usually yields polycrystalline nanowires or fibers, which may lower down the mobility of charge carriers in devices. Compared with the above methods, wet chemical methods are lower cost, higher reproducibility, less hazardous, easier controllability, and thus can be able to large area of preparation. Meanwhile, the nanowires growth temperature is relatively low and compatible with most flexible organic substrates. There are a variety of parameters that can be tuned to effectively control the nanowires length, diameter, distribution and properties of the final product (Gong *et al.*, 2009; Govender *et al.*, 2004). In summary, wet chemical methods have been demonstrated as one of very powerful and versatile techniques for growing 1D ZnO nanowires.

In this chapter, we focus on the 1D ZnO nanostructures that have been prepared by simple hydrothermal self-assembly method and electrospinning. The morphology of ZnO nanostructures were characterized by field emission scanning electron microscopy (SEM). The special reticulate structure assembled by ZnO nanowires exhibits superhydrophobicity with a contact angle of 170° and a sliding angle of 2°. Significant photoluminescence enhancement from ZnO nanowires coated with Ag nanoparticles is observed at 387.6 nm, the ratio of the enhancement reaches 6.6 compared with pure ZnO nanowires. Electrospun ZnO nanowires have also been fabricated into field-effect transistors and sensor devices. The sensors exhibit fast and large response to CO even at room temperature due to highly porous, continuous and compact-grains structures of the electrospun ZnO nanowires.

2. Experimental details

2.1. Hydrothermal self-assembly method

Well-aligned single crystalline ZnO nanowires were prepared from zinc acetate dehydrate in a neutral aqueous solution under hydrothermal conditions. In detail, the Si substrates were first immersed in boiling 98% H_2SO_4 for 10 min and then ultrasonically washed with acetone, ethanol and deionized water, respectively. In order to fabricate well-aligned dispersed ZnO nanowires, a two-step method was used (Wang *et al.*, 2008; Gong *et al.*, 2010): (1) A 10 nm ZnO seed layer was first deposited on a Si substrate by a radio-frequency magnetron sputtering method. A commercially supplied ZnO ceramic plate with a purity of 99.99% was used as a target. The background pressure of the vacuum chamber was 1×10^{-4} Pa. A mixed gas of oxygen and argon with a volume ratio of 1:1 was used as the sputtering gas with a total pressure of 3 Pa. The ZnO seeds were annealed in air for 1hr at 550°C. (2) The hydrothermal growth was carried out at 100°C by immersing the substrates vertically in a mixed aqueous solution containing zinc acetate dehydrate (Zn-AD) and hexamethylenetetramine (He-T). The mixed volume ratio of the two solutions is 1:1, in which the concentration of the two solutions is always the same (i.e. 0.01M/L zinc acetate dehydrate mixed with 0.01M/L hexamethylenetetramine, etc.). The growth time is 12hr. After growth, the sub-

http://dx.doi.org/10.5772/52586

strates were dried in the Far Infrared Drying Oven at 80°C for 5 min (samples 1, 3-6) just after they were immersed in deionized water for 10 seconds. As a comparison, sample 1* is the same as sample 1 except it was not immersed in deionized water. Another substrate was immersed in ethanol for 30min, then in n-Hexane for 90min, drying under natural conditions (sample 2). The reason we chose the different temperature is that the evaporation rate of water at 80°C is almost the same as that of ethanol and n-Hexane at room temperature. Hydrothermal growth and treatment process of ZnO samples are shown in Table 1.The results and the formation mechanism will be discussed in section 3. The morphology of the ZnO film was revealed by SEM images.

samples No.	solution composition	length : diameter	nano-wires density	AA/RA	CA/SA	treatment process
sample 1	Zn-AD 0.01M/L He-T 0.01M/L	104 : 1	$(2.0\pm0.5)\times10^8/cm^2$ (papillary nodes density)	171° / 169.5°	170° / 2°	Immersed in deionized water for 10 seconds, drying in the Far Infrared Drying Oven at 80°C
sample 1*	Zn-AD 0.01M/L He-T 0.01M/L	104 : 1	$(2.9\pm0.5)\times10^8/cm^2$ (papillary nodes density)	169° / 166°	167° / 3°	Without immersed in deionized water, drying in the Far Infrared Drying Oven at 80°C
sample 2	Zn-AD 0.01M/L He-T 0.01M/L	104 : 1	$(2.0\pm0.5)\times10^9/cm^2$	167.5° / 162°	165° / 5°	Immersed in ethanol for 30min, then in n-Hexane for 90min, drying under natural conditions
sample 3	Zn-AD 0.02M/L He-T 0.02M/L	57:1	$(4.0\pm0.5)\times10^9/cm^2$	160° / 151°	157° / 10°	same as sample 1
sample 4	Zn-AD 0.025M/L He-T 0.025M/L	47:1	$(3.1\pm0.5)\times10^9/cm^2$	158° / 142.5°	156° / 18°	same as sample 1
sample 5	Zn-AD 0.04M/L He-T 0.04M/L	17:1	$(1.3\pm0.5)\times10^9/cm^2$	156.5° / 132.5°	153° / 25°	same as sample 1
sample 6	Zn-AD 0.05M/L He-T 0.05M/L	6:1	$(2.4\pm0.5)\times10^8/cm^2$	157° / 145°	154° / 15°	same as sample 1

*The advancing and the receding contact angles (AA/RA), and the contact and the sliding angles (CA/SA) of water droplets on the samples surface (error: ±1°).

Table 1. Hydrothermal solution composition (Zn-AD: zinc acetate dehydrate,andHe-T:hexamethylenetetramine) process and superhydrophobicity of the ZnO nanowires structure

2.2. Electrospinning

Electrospinning has been recognized as an efficient and highly versatile method which can be further developed for mass production of uniform, ultrafine and continuous fibers with nanometer-to-micrometer sized diameter. Up to date, a variety of materials such as polymers, metal oxides, ceramics, metals and carbon have been successfully electrospun into ultrafine fibers mostly from solvent solution(Huang *et al.*, 2003; Tan *et al.*, 2008; Li *et al.*, 2010; Li *et al.*, 2011; Sun *et al.*, 2012; Zhang *et al.*, 2012; Zheng et al., 2012). In this work, ZnO nanowires are also fabricated by calcination of the electrospun fibers of polyvinyl acetate (PVA)/ zinc acetate composite. The processing involved three steps: (1) Preparation of a sol with suitable inorganic precursor and polymer content, and achieving an appropriate viscosity for electrospinning. (2) Spinning of the solution to obtain composite fibers. (3) Calcination of

the composite fibers to remove the polymer coumpounds and obtain the pure oxide nanofibers. In a typical procedure, aqueous PVA solution (2.0 g PVA and 18.0 g deionized water) is dropped slowly into the solution of zinc acetate (2.0 g zinc acetate and 2.0 g deionized water), and the reaction proceeds in a water bath at 90 °C for 2 h.The PVA/zinc acetate composite is cooled down to room temperature, and then the precursor solution is introduced into a syringe with metal spinneret, which is connected to positive electrode of a high-voltage power supply. The spinneret tip-to-collector distance is usually in the range of 8-12 cm, and a dc high voltage in the range of 10-15 kV is necessary to generate the electrospinning, as shown in Fig. 1a. A dense web of PVA/zinc acetate composite wires is then collected on the aluminium foil. Finally the as-electrospun composite wires are calcinated at elevated temperatures (500-600°C) to decompose the PVA organic components, meanwhile the inorganic precursors oxidize and crystallize to form ZnO nanowires.

Fig.1b-e show the morphology evolution of electrospun ZnOwires following hydrolyzation, electrospinning, and calcination processes by our group. After calcination, the average diameter of nanowires appears to be decreased (80-200 nm) attributed to the loss of polymer compounds from the composite fibers and the crystallization of metal oxide. Moreover, the wires often exhibited continuous and compact-grains structures. It reveals that the electrospun wires have a high surface-to-volume ratio. This peculiar morphology enlarges contact area between the fiber and surrounding gas. It may play a pivotal role in the ultra-high sensitivity gas sensor of metal oxide by electrospinning (Kim *et al.*, 2006; Landau *et al.*, 2009).

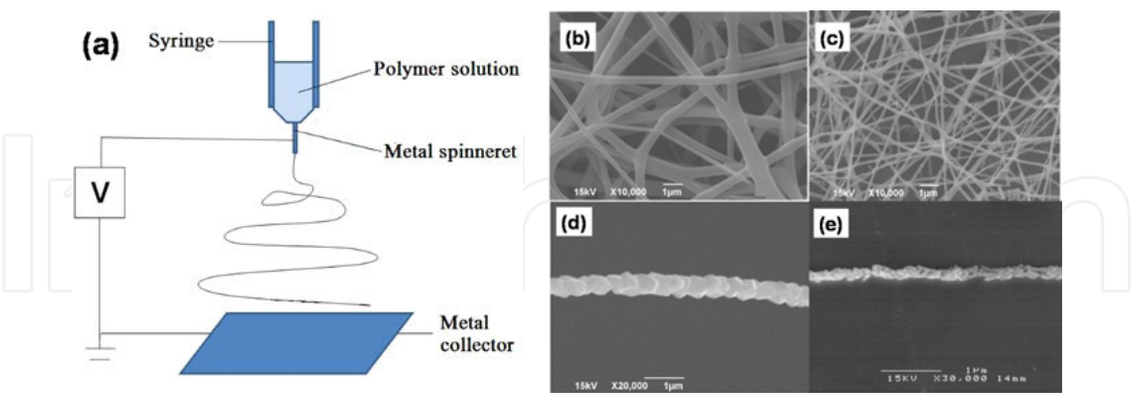

Figure 1. a) Schematic illustration to show polymer nanofibers by electrospinning.SEM images of (b) as-spun PVA/zinc acetate composite fibers and (c) ZnO fibers calcined at 600 °C for 5 h. (d-e) High-magnified SEM images of individual ZnO fibers.

http://dx.doi.org/10.5772/52586

3. Superhydrophobicity of ZnO Nanowires by Hydrothermal Method

3.1. Amalgamation of ZnO Nanowires

Fig. 2 shows the long and slender ZnO nanowires fabricated on the seed layer in the mixed aqueous solution of Zn-AD plus He-T. The ratio of length to diameter is about 104 to 1. Interestingly, the ZnO nanowires in sample 1 self-assembled into reticulate papillary node film (ZnO-RPNF). The growth process of the ZnO-RPNF is illustrated in Fig.3.As shown in Fig.3, during the evaporation and coagulation process of water film on the ZnO nanowires, the ZnO nanowires were aggregated to be a reticulate papillary nodes structure(see Fig.2a). As for the comparison, the ZnO nanowires treated by ethanol and n-Hexane only have a small bending and also remain in their separate condition (see Fig.2c). On the other hand, the nano-wires of the sample 1* soaked in residual water of the reacted solution can also be bended and assembled to a papillary like structure (as shown in Fig.2e), after the water evaporated. Since the solution on the surface of sample 1* was not pure water and the surface tension of the solution is lower, its bending and assembly grade is lower than that of sample 1. The bending and bundling mechanism of vertically aligned ZnO nanowires synthesized by vapor phase deposition method was discussed by other group (Liu *et al.*, 2008). In their report the bending mechanism was attributed to electrostatic interactions between different termination facets with opposite charges. However, the mechanism is different in a liquid phase. Although there are a lot of positive and negative particles in an aqueous solution, a large number of homologous charges would not gather in a given region in a stoichiometric solution. So the EI effect among ZnO nanowires grown by the liquid phase deposition method can be ignored. At 80 °C, the water film on the top of ZnO nanowires evaporates and contracts rapidly to form tiny drops. Therefore, the water has a centripetal surface tension, making the nanowires to be bent and aggregated. On the contrast, the low liquid surface tension (n-Hexane) makes a little bending but not aggregation; the specific reason is explained by the tension junction model.

It is known that the wettability of an ideal surface, expressed with contact angle θ of water droplets, is given by Young's equation:

$$\cos\theta = \frac{\gamma_{SV} - \gamma_{SL}}{\gamma_{LV}} \tag{1}$$

where γ_{SV}, γ_{SL} and γ_{LV} refer to the interfacial surface tensions with solid-vapor, solid-liquid and liquid-vapour, respectively. Young's angle is a result of the thermodynamic equilibrium of the free energy at the solid-liquid-vapor interphase.

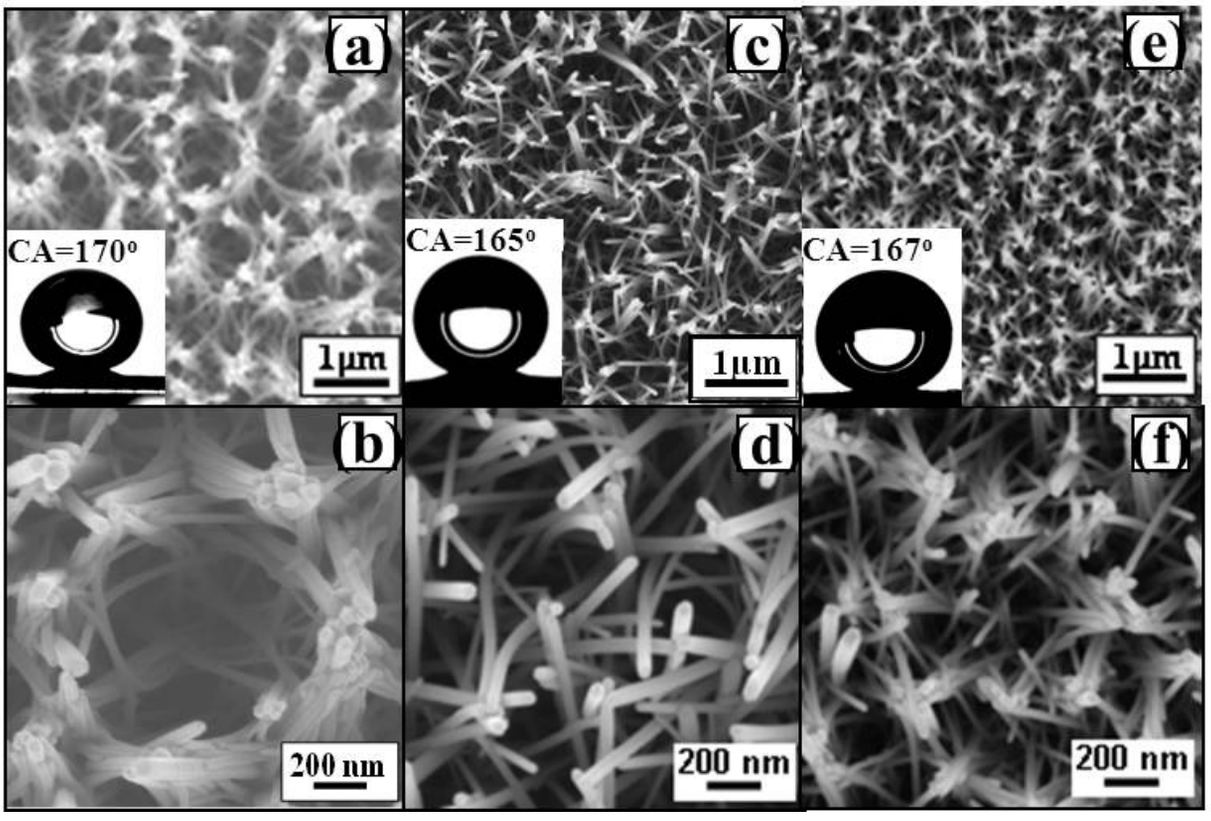

Figure 2. FESEM images of (a) and (b) sample 1, (c) and (d) sample 2, and (e) and (f) sample 1*, where (b), (d) and (f) are the high-magnification for (a), (c) and (e), respectively. The insets show images of droplets that formed on the surface of the different samples during contact angle measurement.

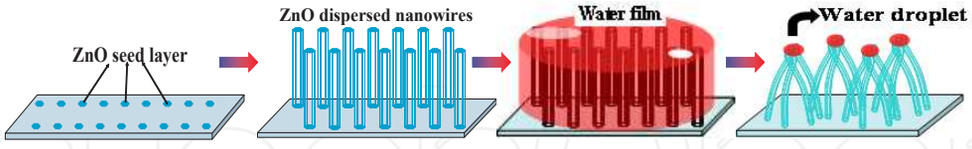

Figure 3. Formation mechanism of the reticulate ZnO film sample 1.

When the ZnO nanowires are free standing in water (or in n-Hexane), it is in a balance state, and there is no force to overcome the elastic deformation force for bending. The model proposed to calculate the magnitude of the forces responsible for the bending is shown in Fig.4. During the drying process, the balance will be broken. The liquid surface tension can be divided parallel to an X-axis factor γ_1 and a Y-axis parallel to the nanowire edge factor γ_2. Note that the γ_2 and the pressure difference $\Delta P=P_L-P_G$ (P_L and P_G are the pressure of the liquid and the atmospheric pressure, respectively) on the droplets arising from the difference in the hollow of the drop cannot let the nanowires be bent. The self-assembling force F_1, parallel to γ_1.F_1 can be obtained from:

http://dx.doi.org/10.5772/52586

$$F_1 = F\sin\theta = \gamma b\sin\theta \tag{2}$$

where$\gamma = \gamma_1+\gamma_2$is the liquid tension, $b=\sqrt{3}d/3$ is the hexagonal side length of the ZnO nanowires (d is the diameter of the ZnO nanowires).

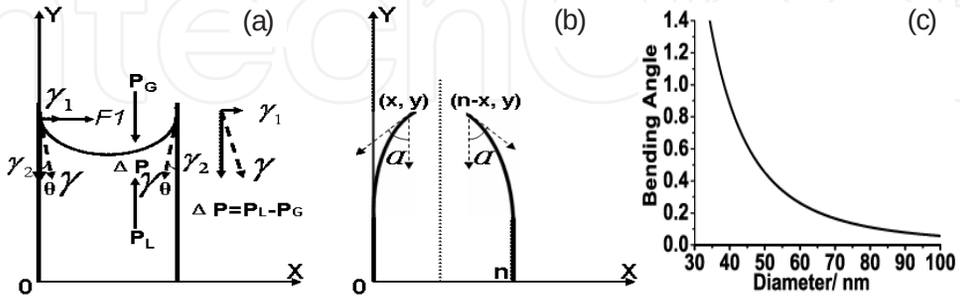

Figure 4. Schematic model of liquid evaporation induced change of the bending angles between two ZnO nanowires, where (a) indicates the initial state of water with two nanowires system; (b) is any intermediate state during the bending process.The bending angle vs. the nanowires diameter is as shown in (c).

To simplify the case, we just consider the liquid surface tension between two nanowires. The initial state for two nanowires with lengths T is shown by Fig.4a, where the two nanowires lengths are defaulted as the same. The self-assembling parallel tension pressed on ZnO nanowires with water F_w and with n-Hexane F_h can be expressed as:

$$\frac{F_w}{b} = \gamma_w \sin\theta_w \tag{3}$$

$$\frac{F_h}{b} = \gamma_h \sin\theta_h \tag{4}$$

whereγ_w and γ_h are the surface tension of water and n-Hexane, θ_w and θ_h are the contact angle of water and n-Hexane on a ZnO nanowire, respectively. γ_w=62.61mN/m at 80°C, and γ_h=18.4 mN/m, θ_w =33°, θ_h= 0° at 20 °C, respectively. From the calculation, we observe F_w=34.1bmN/m, and F_h=0. For sample 1, the average diameter of the nanowires d is 42.3 nm. Therefore, the parallel surface tension of water is F_w= 8.33×10^{-10} N.

A tension junction model as shown in Fig.4 is used to estimate the minimum parallel surface tension which is necessary to make two nanowires contact each other. For simplicity, we assumed two symmetric flexible nanowires separated by a distance n. Furthermore, we approximated the parallel surface tension applied on the top of the nanowire. The dependence of the lateral displacement x perpendicular to the nanowire on the elastic bending force applied at the top is given as (Song *et al*., 2005):

$$F_{elastic} = \frac{3EI}{T^3} x \tag{5}$$

where T, E and I are the length, Young's modulus and moment of inertia of the ZnO nanowire, respectively. The moment of inertia of a hexagonal-cross-section nano-wire can be expressed as $I = 5\sqrt{3}d^4/144$. To make these two symmetric wires a contact at $x=n/2$, the parallel surface tension has to be larger than the bending force for $n/2$ displacement.

Reported values for elastic modulus of ZnO nanostructures vary greatly depending on experimental methods and nanostructure dimensions. For example, Wang *et al.* measured the elastic modulus of vertical ZnO nanowires on sapphire to be 29±8 GPa based on atomic force microscopy (Song *et al.*, 2005). Their nanowires had an average diameter of 45nm and length ranging from 0.277 to 0.638 μm. By manipulating the vertical ZnO nanowires with an atomic force microscopy tip, Hoffmann *et al.* measured an average elastic modulus of about 100 GPa for 250 nm diameter ZnO nanowires (Hoffmann *et al.*,2007). Huang *et al.* used transmission electron microscopy to measure the elastic bending modulus of ZnO nano-wires via electric-field-induced resonant excitation and obtained a mean elastic modulus of ~58 Gpa (Huang *et al.*, 2006). In particular, they measured the elastic modulus of 48.9GPa from a ZnO nanowire with diameter of 43 nm and length of 4.77 μm, which is similar to that (d=42.3 nm, T=4.41 μm) of sample 1. If choosing E=50 Gpa while n = 224 nm based on the nanowires density in Table 1 to calculate the elastic bending force, we therefore obtain

$$F_{elastic} = 3.77 \times 10^{-11} (N) \tag{6}$$

For sample 1 the water's parallel surface tension F_w= 8.33×10^{-10} (N) is about 22 times more than $F_{elastic}$. Therefore, the surface tension of deionized water is big enough to let two or more nanowires bundling together to form the reticulate papillary nodes structure. Note that although the parallel surface tension of n-Hexane is F_h = 0, after the substrate was immersed in the n-Hexane, a little bending of the nanowires of sample 2 still happened (see Fig.2d), due to that the residual water in solution cannot be thoroughly removed.

As shown in Fig.4b, the angle α (the angle between the Y-axis and the tangent at the nanowire tip) is used for defining any intermediate state during the bending process. The relationship between the F_1 (required to overcome the bending-induced elastic energy, for water: $F1 = F_w$) and the bending angle is $\alpha = F_1 T^2/2EI$ (Hibbeler, 1997). Since there is no other external force in X-axis, the bending forces experienced by the two nanowires must be equal. To simply obtain the relation between the bending angle and the nanowires diameter, we assumed that the parallel surface tension of water, Young's modulus and the length of ZnO nanowires are constant as F_w=8.33×10^{-10}N, E=50 GPa and T=4.41 μm, respectively. The curve in Fig.4c is the bending angle as a function of the nanowires diameter of samples 1, 3-6. The bending angle decreases sharply as the diameter increases. The bending will be faded out as the diameter increases enough.

http://dx.doi.org/10.5772/52586

All obtained ZnO samples are wurtzite structure, as shown by SEM images in Figs.2 and 5. Fig.2a is SEM top image of the reticulate ZnO film, exhibiting the homogeneous micro/nanostructures on a large scale, Fig. 2b is the high magnification. The top inset of Fig.5a shows a selected area electron diffraction pattern of the ZnO-RPNF that confirms the single crystalline property of the ZnO nanowire. The average reticulate width and density, and the factors for the surface roughness of the reticulate ZnO film, are also determined from top-view SEM image. The reticulate ZnO nanowires (sample 1) with the diameters from 20 to 60 nm (the average is 42.3 nm) are even distributed on the whole substrates. The density of surface nodes (top of the nanowire or the papillary) was decreased via assembly of about ten nanowires to one papillary node. In our data, the density was changed from $(2.0\pm0.5)\times10^9/cm^2$ to $(2.0\pm0.5)\times10^8/cm^2$ (see Table1).

It is also found in Table 1 that the nanowires' density decreased as the zinc acetate dehydrate concentration increased, due to the nanowires fusing easily together in their growth process. However, as the concentration is very low, the density of nanowires is also lower which is due to the fact that some seed particles did not grow into the longer nanowires, just like sample 1.

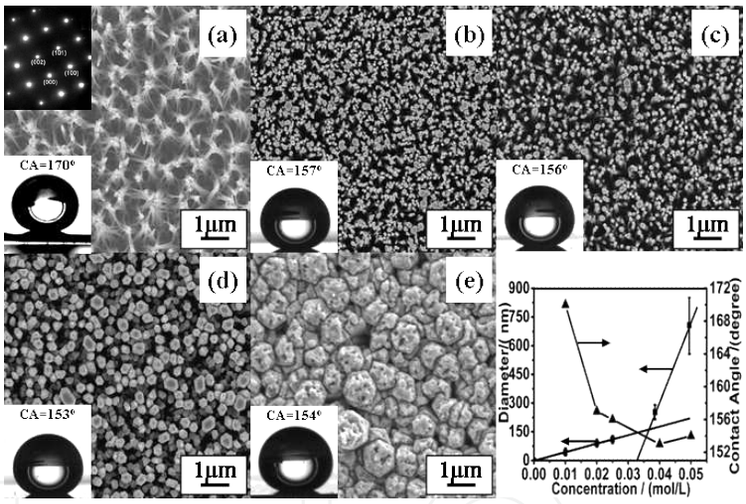

Figure 5. The surface FESEM images of ZnO nanowires of (a) sample 1, (b) sample 3, (c) sample 4, (d) sample 5, and (e) sample 6. The insets show images of the droplets that formed on the surface of the different samples during the contact angle measurement. The top inset of (a) shows the selected area electron diffraction pattern of the ZnO-RPNF that confirms the single crystalline ZnO nanowire. Variation of the ZnO nanowire's diameter and water contact angle measured on the surface of different samples (sample 1, samples 3 to 6) as a function of the concentration of hexamethylenetetramine and zinc acetate dehydrate solution is shown in (f), with the variation range of the nanowires diameter indicated by the error bars.

The general trend was that as ZnO nanowires had a larger aspect ratio and smaller diameter, they were more susceptible to assemble reticulate film with papilla structure. For example, for any given diameter and density, nanowires would not overcome their own elastic modulus and assemble, but assembling by liquid surface tension would become prominent as nanowires grew longer and thinner. The assembling degree of nanowires in Fig.5 was consistent with this general trend. The aspect ratio and diameter in Fig.5a-e were 104:1 and

42.3nm, 57:1 and 88.8nm, 47:1 and 110.3nm, 17:1 and 246.3nm, and 6:1 and 698.5nm, respectively. As expected the degree of assembling was largest in Fig.5a and smallest in Fig.5e.The diameter *d* variation as functions of the concentration *c* is shown in Fig.5f. The function is expressed as *d*=4440*c* (nm) when the concentration is lower than 0.04M/L, indicating a growth mode for single nano-wire. However, as the concentration increases to 0.04M/L and 0.05M/L, the variation function changes to d=45220c-1562.5(nm). The slope of which is 10 times more than the former.This could be attributed to the merging between the nanowires. As the solution concentration increases, the diameters of the nanowires increase while the distance between them decreases. When the diameters reached a certain value, the spaces between the nanowires became zero, resulting in the amalgamation of nanowires.

3.2. Superhydrophobicity

Wettability of a solid surface has attracted much attention during the past decades, due to its broad technological applications and fundamental researches. A direct expression of the wettability is the contact angle of a water droplet on the surface. Surfaces with very high water contact angles particularly greater than 150° are usually called superhydrophobic surfaces, which have been extended to more applications, such as self-cleaning materials, anti-fog, anti snow, fluid microchips and microreactors (Richard *et al.*, 2002; Erbil *et al.*, 2003; Jiang *et al.*, 2004; Chen *et al.*, 2006).

The obtained ZnO-RPNF was superhydrophobic (see the insert of Fig.2a). The water contact angle is measured to be 170±1°, and the water volume is 10μL. The contact angle hysteresis, which is the difference between the advancing and receding angles, is measured to be less than 2°. The water droplets roll off of the substrate at a sliding angle of less than 2°. The water contact angle on the plane ZnO thin film modified via heptadecafluorodecyltrimethoxysilane (HTMS) was about 114±1°, which is near to the maximum 119° (Nishino *et al.*, 1999). The largest variance in the contact angle is due to the surface roughness. These data suggest that the predominant contribution to the large contact angle is the reticulate papillary nodes structure. Furthermore, the obtained ZnO-RPNF maintains superhydrophobic properties even after ambient environment for three months, showing their favorable stability. This is very important for extending the practical applications of ZnO materials.

The basic effect of the surface structure and chemistry on superhydrophobicity has been elucidated by Wenzel (Wenzel, 1936) and Cassie (Cassie and Baxter, 1944) models. Wenzel's model hypothesizes that the liquid completely penetrates into the troughs of the surface texture. Cassie's model is based on the assumption that the liquid drop doesn't fill the troughs of the rough surface but sits on a composite surface composed of solid material and air. Both the Wenzel and Cassie models have put emphasis on the geometrical structure of a solid surface as an important factor in determining the hydrophobicity. The trapping of air in the surface troughs causes an increase in the water contact angle according to Cassie-Baxter'sequation (Jiang *et al.*, 2004).

$$\cos\theta^* = f_1 \cos\theta_1 + f_2 \cos\theta_2 \tag{7}$$

http://dx.doi.org/10.5772/52586

$$f_1 + f_2 = 1 \tag{8}$$

where $\theta^*$is the contact angle on HTMS coating the rough surface of reticulate ZnO film with papillary nodes, θ_1 and $\theta_2$are the contact angles on HTMS coating the plane ZnO film and air, respectively; f_1 and $f_2$are the fractions of the papillary nodes' end surface and of the trapped air on reticulate ZnO film. Here, θ_2 is 180°. Substituting θ_2 and (8) into equation (7) will lead to:

$$\cos\theta^* = f_s \cos\theta_e + f_s - 1 \tag{9}$$

here f_s is the fractions of the papillary nodes end surface, and $\theta_e$is the contact angle on HTMS coating ZnO plane film (θ_e=114°).

We notice from eq. (8) that if the reticulate ZnO film with papillary nodes has a very low f_s, a superhydrophobic thin film with a high water contact angle could be fabricated. The value of f_s is estimated by the SEM experiments. As mentioned above, the average diameter of one nanowire is 42.3 nm, and the growth density D is about (2.0±0.5)×10^9 per square centimeter by a mass of statistic.Due to the top of ZnO nanowire being hexagonal, the nanowire diameter d and the growth density D is 42.3nm and 2.0×10^9 per square centimeter, respectively. The f_s is obtained as:

$$f_s = (2 \times \frac{\sqrt{3}}{12} d^2 + \frac{d^2}{2\cos 30^\circ}) D = \frac{\sqrt{3}}{2} d^2 D = 0.031 \tag{10}$$

Substituting (10) into eq. (9) will lead to:θ^*=169°. The calculated value is in good agreement with the experimental datum 170°±1° of sample 1. However, the experimental data of sample 1* and sample 2 are 167° and 165° (see Table 1 and Fig.2), respectively. We know from the Cassie model that the air trapped in the surface structure plays an important role for the surface with a larger contact angle. The reticulate structure may serve as a means of trapping sufficient air for larger contact angles to be exhibited. A reticulate papillary node on sample 1 is the assembly of about ten nanowires on average, and the wires bending with a spiral line structure before bundling together at the wires' top. This makes the nano-papillary nodes distribute with circularity and forms a larger column-like micro space (see Fig. 2b). This micro/nano complex structure is closed to the bionic lotus-leaf-structure and much in line with the Cassie model. Nevertheless, the papillary nodes of sample 1* are bended simply by seven nanowires; there is no larger mirco space as that in sample 1. Therefore its superhydrophobicity is lower than that of sample 1. As a comparison, the contact angle of sample 2 is the lowest, because it has fewer or no reticulate papillary nodes.

The contact angle on the surface of different samples formed by nanowires tends to decrease as the surface density of nanowires and the width between them decrease (see Table 1 and Fig.5). As represented in Fig.5f, the contact angle decreases from 170° (sample 1) to 154°

(sample 5). This result is consistent with that of the superhydrophobicity behavior determined by the density of the nanowires and the space between them (Borras *et al.*, 2008). Note that although the nanowires fused together, the contact angle on the surface of sample 6 (Fig.5e-f) is not the minimum, due to the protuberance on the surface.

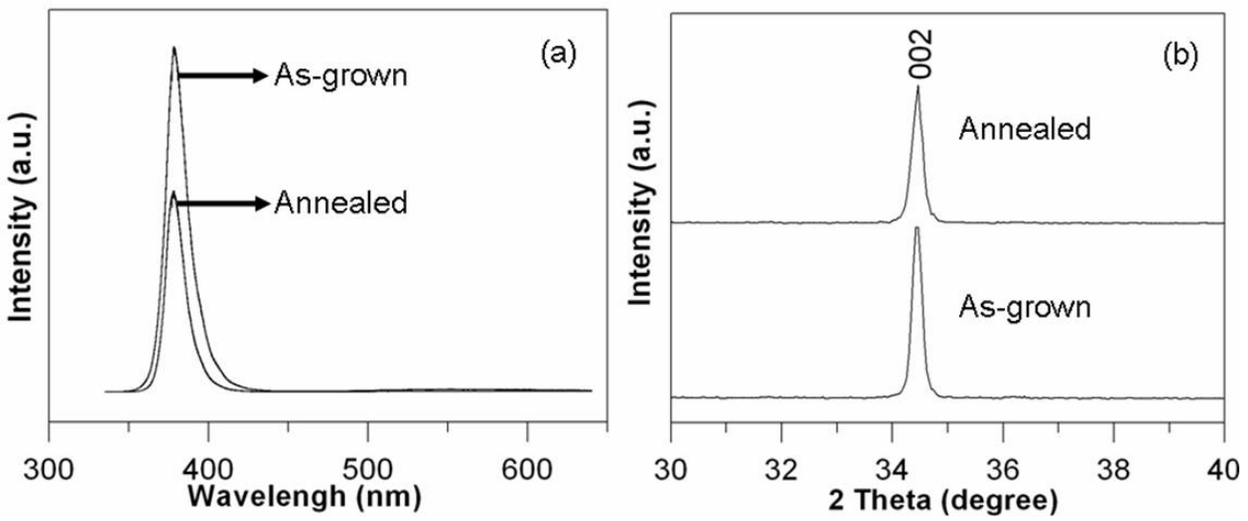

Figure 6. Room-temperature photoluminescence spectra (a), and XRD patterns (b) of ZnO as-grown and annealed at 550 °C for 1h.

4. Photoluminescence of ZnO nanowires via hydrothermal method

ZnO exhibited a wide band gap at room temperature with a large exciton binding energy, which is suitable for effective ultraviolet emission. However, due to the poor crystalline quality of the nano materials, *i.e.* high density of structure defects, the ultraviolet emission of nano-scaled ZnO is liable to be quenched and only defect emission in visible region is detected (Kong *et al.*, 2001). This deficiency hinders process for the application of ZnO in optoelectronic and lasing devices. Therefore, improving the crystal quality of ZnO by synthetic processing and realizing ultraviolet emission and lasing are still major challenges.

The study of photoluminescence is a favorable way to evaluate both ZnO optical properties and its structural defects. Normally, ZnO nanostructures can exhibit ultraviolet emission resulting from the recombination of free excitons and visible emission due to some structural defects(Djurisic and Leung, 2006). Fig.6a gives the room-temperature photoluminescence spectra of ZnO nanowires growing at low temperature of 50 °C by hydrothermal method with as-grown and annealed, in which only ultraviolet emission peaks centered at about 378.5 nm dominate, while the well-known broader emission situated in the blue-red part of the visible spectrum could not be observed (Wang *et al.*, 2007). This result can be attributed to the fine crystallization of the ZnO nanowires. The ultraviolet emission intensity of the as-grown nanowires is better than the annealed one, which indicates the annealing process de-

http://dx.doi.org/10.5772/52586

creased the crystal quality of ZnO just as the XRD showed Fig.6b. Therefore, ZnO nanowires growing at lower temperature by hydrothermal method have huge potential to fabricate high crystalline quality and good ultraviolet luminescence devices.

The ultraviolet emission intensity of ZnO nanowires is very important in lasing devices. As mentioned above, the intensity can be enhanced by improving crystalline quality of ZnO nanowires. In addition to amending their own quality, surface plasmons or localized surface plasmons of various noble metals also can be used to realize ZnO nanowires photoluminescence enhancement. You's group sputtered ZnO film on Si (001) substrate which had already been coated with 100 nm Ag film previously, and the ultraviolet emission of the composite is found to be greatly enhanced (You *et al.*, 2007). Xiao *et al.* have also found enhancement of near-band-emission of ZnO by coating a layer of Ag implanted silica film(Xiao *et al.*, 2010).

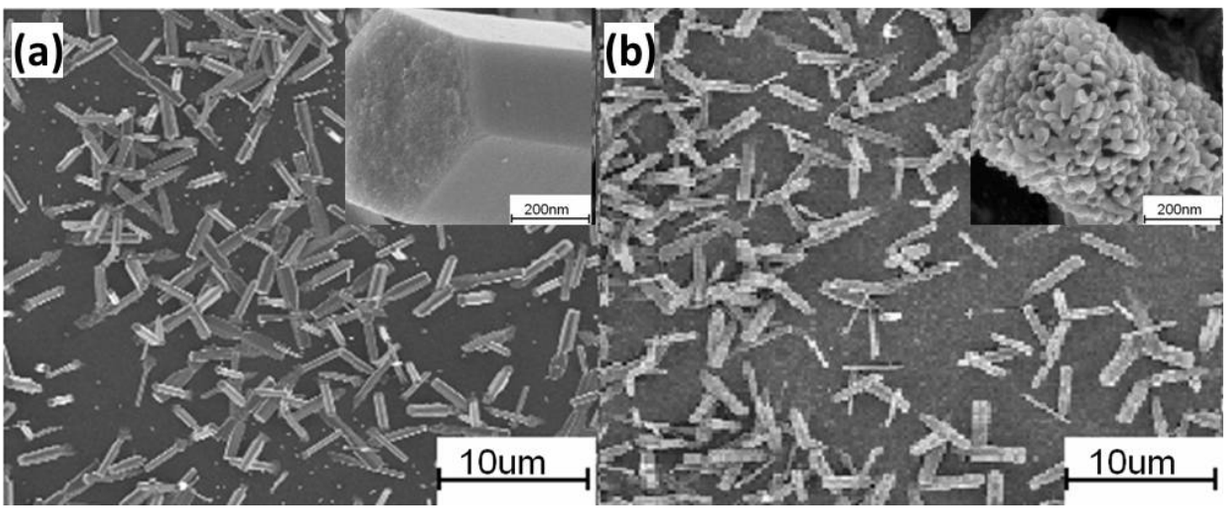

Figure 7. SEM images of (a) ZnO nanowires non-coating and (b) ZnO nanowires coated with separated Ag nanoparticles.

ZnO nanowires grown by the two-step method as mentioned above and annealed in air at 400°C for 1 hr in order to eliminate the defects in ZnO. Then, 40 nm Ag deposited on the ZnO nanowire arrays surface by the radio-frequency magnetron sputtering method at room temperature. Fig.7 shows SEM images of ZnO nanowires non-coating and coated with Ag nanoparticles on the surface. The nanowires, dispersed, lay on the substrate, 4-6 μm in length and 400-600 nm in diameter, and formed a perfect hexagonal structure. It is clear that the nanowires in Fig.7 show almost no difference-either in size or density. There is apparently a layer of 40-50 nm Ag nanoparticles on the nanowires in the inset image of Fig.7b, and the roughness of the surface of the metal is quite high.

The photoluminescence spectra of the ZnO nanowires non-coating and coated Ag nanoparticles are shown in Fig.8. The spectrum of the ZnO nanowires is shown as curve *a*. The peak position at 381.6 nm with 87 meV full width at half maximum, this was attributed to FX-1LO (Shan *et al.*, 2005; Hamby *et al.*, 2003). The emission for the visible light mostly caused by the defect in

ZnO is very week, indicating good quality of the ZnO nanowires. Accordingly, the ZnO nanowires are one of the good optional materials for ultraviolet lasing devices. Curve *b* in Fig.8 is the spectrum of ZnO nanowires coated with 40 nm Ag nanoparticles, showing a greatly enhanced photoemission. The ratio enhancement reaches 6.6 compared with pure ZnO nanowires. Therefore, the photoluminescence of the Ag/ZnO nanowires is apparently stronger than that of ZnO nanowires non-coating because of the intensive coupling between ZnO nanowires and localized surface plasmons of Ag nanoparticles (Lü *et al.*, 2008), which informs us of a good orientation for the composite of metal and semiconductor as a laser source material.

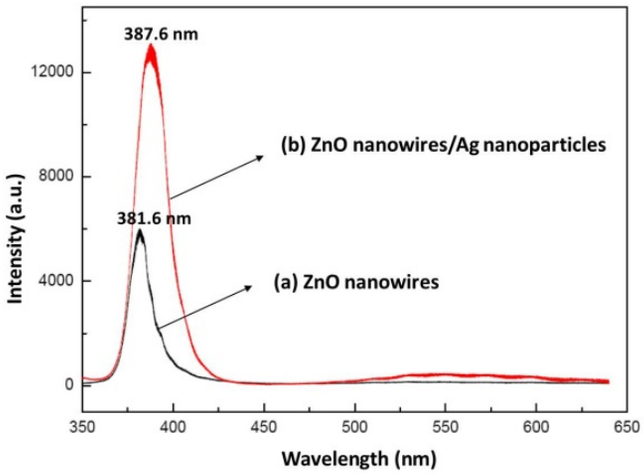

Figure 8. Photoluminescence spectra of (a) ZnO nanowires non-coating and (b) ZnO nanowires coated with 40 nm Ag nanoparticles.

5. Electrical and sensing properties of ZnO nanofibers via electrospinning

Besides hydrothermal self-assembly method, ZnO nanowires were also fabricated by calcination of electrospun poly(vinyl alcohol)/zinc acetate precursor wires at 600 °C for 5 h, as shown in Fig. 1. Raman spectroscopy and XRD were used to confirm the formation of a pure ZnO phase in the nanowires after calcination treatment. Fig.9a shows the clear phonon modes of the wires calcined at 600 °C: the two phonon modes at 439 and 582 cm^{-1} could be assigned to E_2 (high) and A_1 (LO), separately; the phonon mode at 325 cm^{-1} is a second-order phonon, which generally originates from the zone-boundary phonons of $2E_2$ (low). This Raman spectrum is typical for pure, polycrystalline ZnO. Fig.9b gives the XRD pattern for the as-spun fibers after calcinations at 600 °C for 5 h. A clear diffraction pattern is shown, and nine reflection peaks appear at 2θ=31.9° (100), 34.6° (002), 36.5° (101), 47.7° (102), 56.8° (110), 63.1° (103), 66.5° (200), 68.1° (112), and 69.2 (201). It agrees well with the JCPDS card, No. 89-1397 for pure ZnO, confirming the as-prepared product is pure ZnO nanowires after calcination at that temperature.

http://dx.doi.org/10.5772/52586

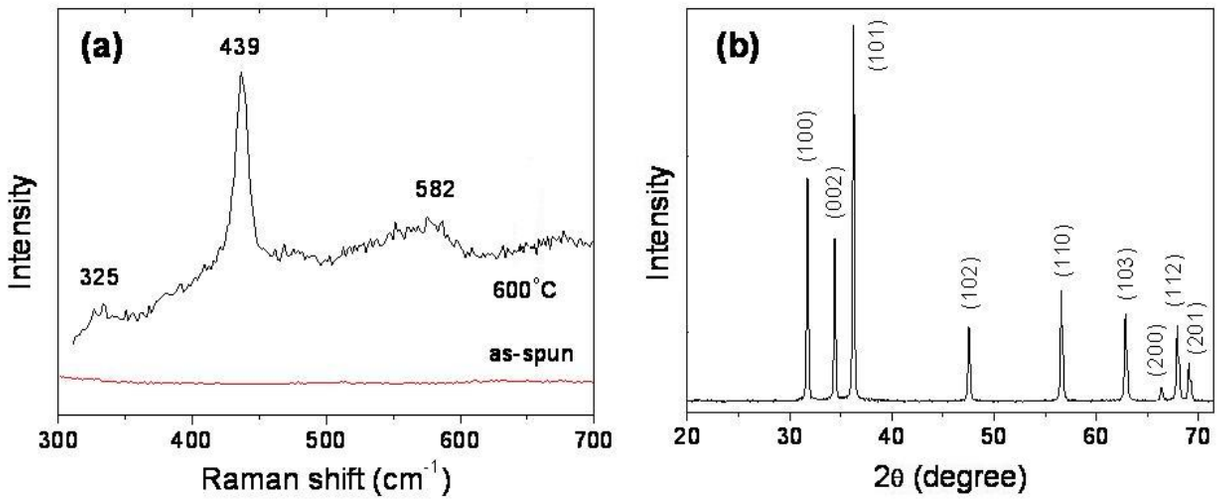

Figure 9. a) Raman spectra of as-spun PVA/zinc acetate nanowires before and after calcinations at 600 °C for 5 h in atmosphere. (b) XRD pattern of the ZnO nanowires.

To fabricate ZnO nanowire-based field-effect transistor or gas sensor device, SiO_2/Si chip with pre-patterned Au electrode arrays via traditional e-beam lithography technology was used as collector to collect PVA/zinc acetate nanowires. The collecting time was about 5 s. The chip was then calcined at 600 °C for 4 h to obtain ZnO nanowires device. As shown in Fig. 10a, the square Au electrodes have a side length of 50 μm, and a long ZnO wire is clearly deposited across the electrodes. In another device, PVA/zinc acetate nanowire yarns were deposited on SiO_2/Si chip by a two-parallel-electrode method or gapping method (Tan *et al.*, 2008). After calcination of the chip at 600 °C for 4 h, two electrodes made of silver paste were attached onto the ZnO nanowire yarns, as shown in Fig. 10b.

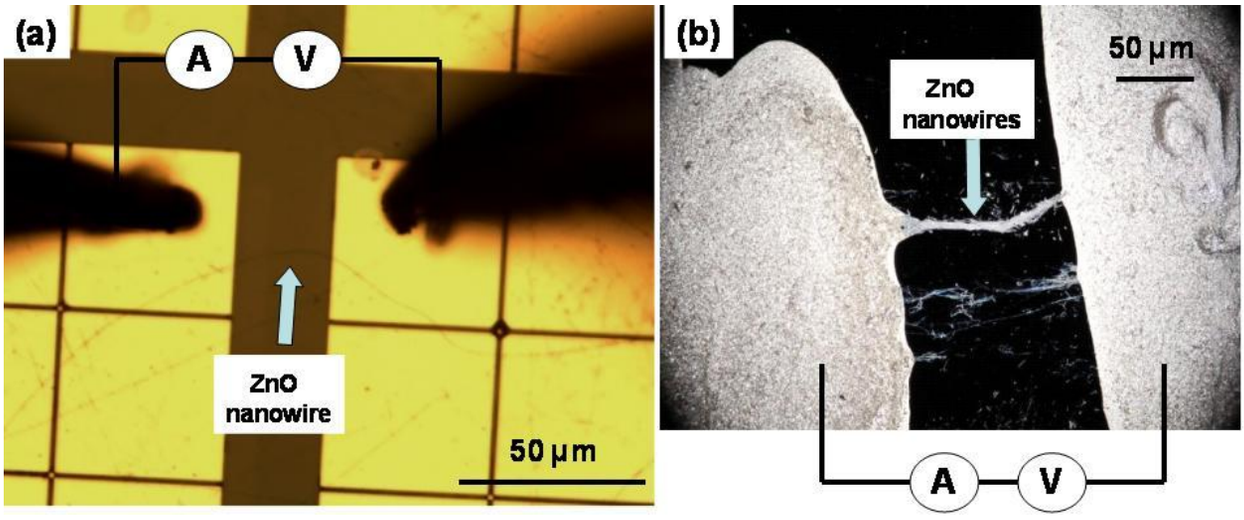

Figure 10. a) Optical image of an individual electrospun ZnO nanowire measured by two-probe method; (b) Optical image of a bundle of electrospun ZnO nanowires and attached Ag paste electrodes.

Current-voltage (I-V) curves were performed on the single ZnO nanowire device by using two-metal-microprobe testing platform. Fig.10a shows the optical picture that two metal microprobes were pressed directly on the square Au electrodes. The scanning voltage was applied from -20 to 20 V with a step of 0.1 V. At the same time the current corresponding to each applied voltage was measured. Fig.11a shows the I_{ds}-V_{ds} characteristic curves of the single ZnO nanowire at dark and under illustration. It is evident that the electrospun ZnO nanowire has a very large resistance (~$1.4x10^{10}\Omega$) at dark: under bias voltage of 20 V, the current is only about 1.4 nA. But the current increases sharply under illustration. The current can reach 19.8 nA (20 V bias) when the color temperature of illustration is 2900 K. In addition, the Si substrate was used as a back gate to measure gate effect of this ZnO nanowire device. As shown in Fig. 11b, higher source-drain currents were measured when positive gate voltages V_g were applied. It indicates that the electrospun ZnO nanowire is an intrinsic *n*-type semiconductor. The above results are in accordance with that obtained from other ZnO nanowire field-effect transistor devices fabricated by the chemical vapour deposition or hydrothermal self-assembly method.

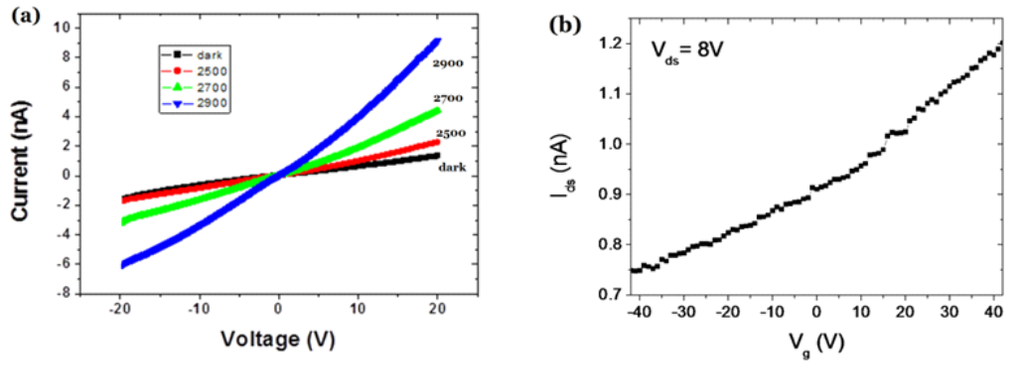

Figure 11. (a) Current-voltage (I_{ds}-V_{ds}) characteristic curves of an individual ZnO nanowire (as shown Fig.10a) at dark and under illustration. The illustration intensity is represented by color temperature of 2500, 2700and 2900 K. (b) Source-drain current (I_{ds}) versus gate voltage (V_g) at V_{ds}=8 V for the same ZnO nanowire device.

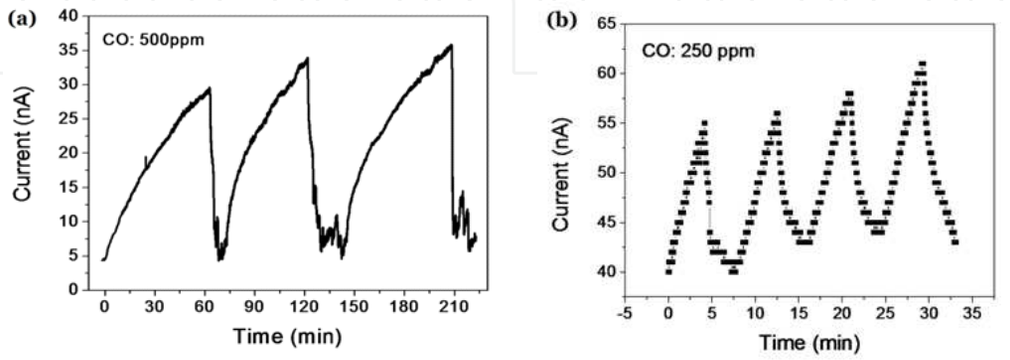

Figure 12. Response of the gas sensor based on (a) an individual ZnO nanowire, and (b) a bundle of ZnO nanowires towards 500 or 250 ppm CO as a function of time at room temperature. The applied voltage is 20 V.

http://dx.doi.org/10.5772/52586

In addition to transistors and photodetectors, ZnO has been proved to be a kind of highly sensitive material for the flammable or toxic gas detection, such as H_2, CO, NO, or ethanol (Zeng *et al.*, 2009; Krishnakumar *et al.*, 2009). To improve the sensing performance of the gas sensors, usually the ZnO nanowires were doped with metal or metal-oxide to form surface depletion layer, and thus enhance the sensing properties (Li *et al.*, 2012; Liu *et al.*, 2009; Pan *et al.*, 2001). Moreover, a heater was necessary for most of the gas sensors to work at high temperatures of about 200-400°C, which leads to the sensor complex and high-cost. In this work, since the electrospun ZnO nanowires exhibit continuous and compact-grains structures and thus have a high surface-to-volume ratio, gas sensing measurements of nanowire devices based on one single ZnO nanowire and one bundle of ZnO nanowires were carried out. As shown in Fig. 12, the ZnO nanowires exhibit rapid, apparent response when exposed to 500ppm or 250 ppm CO even at room temperature. Since the gas response can be defined as the ratio: $S \approx |R_{air}-R_{gas}|/R_{air}$, where R_{air} and R_{gas} are the resistance of the sensor in dry air and in the test gas, separately, Fig. 12 indicates that the gas response can reach 500 % in 60 min towards 500 ppm CO or 26% in 5 min towards 250 ppm CO.

The ZnO carbon monoxide gas sensing can be explained by the chemical reaction between the active gas and oxygen ion adsorption on the surface of ZnO. In air atmosphere, oxygen molecules are adsorbed onto the surface of the ZnO sensor to form O^- or O^{2-} ions by attracting electrons from the conduction band of the ZnO. Under carbon monoxide atmosphere, the CO gas reacts with oxygen ion molecule on the surface and gives back electrons into the conduction band, thereby lowering the resistance of ZnO sensors. ZnO nanostructures exhibit sensor response higher than the bulk; this can be simply explained by the effect of the surface-to-volume ratio. In the present case, the fast and large response to CO at room temperature can be ascribed to small nanocrystal size, high surface area and high porosity of the resultant ZnO nanowires.

6. Summary

ZnO nanostructures have drawn great attention for their wide applications in electronic, optical, optoelectronic, sensing, catalysis, hydrophobic surface modification, and energy harvesting devices (Xu and Wang, 2011). In this chapter, our recent results in synthesis, physical properties and sensor applications of ZnO nanowires are presented. Crystalline ZnO nanowires and polycrystalline ZnO nanofibers are prepared by simple hydrothermal self-assembly method and electrospinning, respectively. The surfaces of ZnO nanowires thin film after surface modification are superhydrophobic with a contact angle of 170° and a sliding angle of 2°. As one of the best optional materials for ultra-violet laser devices, ZnO nanowires grown by hydrothermal method have good photoluminescence properties and photoluminescence enhancement at 387.6 nm by coating a layer of Ag nanoparticles. ZnO nanowires with porous fibrous morphology fabricated via electrospinning have specific surface approximately one to two orders of the magnitude larger than flat films, making them excellent candidates for potential applications in gas sensors. For example, the granular ZnO

nanowires exhibit fast and large response to CO even at room temperature. Further studies are in progress to improve the performance of these nanodevices.

Acknowledgments

This work was supported by the National Natural Science Foundation of China (Grant Nos.: 11074138, 50872129 and 11004114), the Taishan Scholars Program of Shandong Province, the Natural Science Foundation of Shandong Province, China for Distinguished Young Scholars (Grant No.: JQ201103), and the National Key Basic Research Development Program of China (973 special preliminary study plan) (Grant No.: 2012CB722705).

Author details

M.G. Gong[1,2], Y.Z. Long[1,3,4], X.L. Xu[2], H.D. Zhang[1] and B. Sun[1]

1 College of Physics, Qingdao University, People's Republic of China

2 Department of Physics, University of Science and Technology of China, People's Republic of China

3 Key Laboratory of Photonics Materials and Technology in Universities of Shandong, Qingdao University, People's Republic of China

4 State Key Laboratory Cultivation Base of New Fiber Materials and Modern Textile, Qingdao University, People's Republic of China

References

[1] Borras, A.; Barranco, A.; Gonzalez-Elipe, A. R. (2008). Reversible superhydrophobic to superhydrophilic conversion of Ag@TiO_2 composite nanofiber surfaces. *Langmuir*, Vol. 24, June 2008, pp. 8021-8026, ISSN: 1520-5827.

[2] Cao, B. Q.; Lorenz, M.; Rahm, A.; von Wenckstern, H.; Czekalla, C.; Lenzner, J.; Benndorf, G.; Grundmann, M. (2007). Phosphorus acceptor doped ZnO nanowires prepared by pulsed-laser deposition. *Nanotechnology*, Vol. 18(45), Oct. 2007, pp. 455707-455711, ISSN: 1361-6528.

[3] Cassie, A. B. D.; Baxter, S. (1944). Wettability of porous surfaces. *Trans. Faraday Soc.*, Vol. 40, June 1944, pp. 546-551, ISSN: 0014-7672.

[4] Chen, Y. B.; Ambade, A. V.; Vutukuri, D. R.; Thayumanavan, S. (2006). Self-assembly of facially amphiphilic dendrimers on surfaces. *J. Am. chem. Soc.*, Vol. 128(46), Nov. 2006, pp. 14760-14761, ISSN: 0002-7863.

[5] Chiou, W. T.; Wu, W. Y.; Ting, J. M. (2003). Growth of single crystal ZnO nanowires using sputter deposition. *Diamond and Related Materials*, Vol. 12(10-11), 2003, pp. 1841-1844, ISSN: 0925-9635.

[6] Djurisic, A. B.; Leung, Y. H. (2006). Optical properties of ZnO nanostructures. *Small*, Vol. 2, Aug. 2006, pp. 944-961, ISSN: 1613-6829.

[7] Erbil, H. Y.; Demirel, A. L.; Avci, Y.; Mert, O. (2003). Transformation of a simple plastic into a superhydrophobic surface. S*cience*, Vol. 299, Feb. 2003, pp. 1377-1380, ISSN: 0036-8075.

[8] Gong, M. G.; Xu, X. L.; Yang, Z.; Liu, Y.; Lü, H.; Lü, L. (2009). A reticulate superhydrophobic self-assembly structure prepared by ZnO nanowires. *Nanotechnology*, Vol. 20(16), Apr. 2009, pp. 165602-165608, ISSN: 1361-6528.

[9] Gong, M. G.; Xu, X. L.; Yang, Z.; Liu, Y. S.; Liu, L. (2010). Superhydrophobic surfaces via controlling the morphology of ZnO micro/nano complex structure. *Chin. Phys. B*, Vol. 19(5), May 2010, p. 056701, ISSN: 1674-1056.

[10] Goris, L.; Noriega, R.; Donovan, M.; Jokisaari, J.; Kusinski, G.; Salleo, A. (2009). Intrinsic and doped zinc oxide nanowires for transparent electrode fabrication via low-temperature solution synthesis. *Journal of Electronic Materials*, Vol. 38(4), 2009, pp. 586-595, ISSN: 1543-186X.

[11] Govender, K.; Boyle, D. S.; Kenway, P. B.; O'Brien, P. (2004). Understanding the factors that govern the deposition and morphology of thin films of ZnO from aqueous solution. *Journal of Materials Chemistry*, Vol. 14(16), June 2004, pp. 2575-2591, ISSN: 1364-5501.

[12] Hamby, D. W.; Lucca, D. A.; Klopfstein, M. J.; Cantwell, G. (2003). Temperature dependent exciton photoluminescence of bulk ZnO. *J. Appl. Phys.*, Vol. 93, 2003, p. 3214, ISSN: 1089-7550.

[13] Heo, Y. W.; Varadarajan, V.; Kaufman, M.; Kim, K.; Norton, D. P.; Ren, F.; Fleming, P. H. (2002). Site-specific growth of ZnO nanorods using catalysis driven molecular-beam epitaxy. *Applied Physics Letters*, Vol. 81(16), Aug. 2002, pp. 3046-3048, ISSN: 1616-3028.

[14] Hibbeler, R. C. Mechanics of Materials, 3rd ed. (1997, Prentice-Hall, Engle-wood Cliffs, NJ)

[15] Hoffmann, S.; Ostlund, F.; Michler, J.; Fan, H. J; Zacharias, M.; Christiansen, S. H.; Ballif, C. (2007). Fracture strength and Young's modulus of ZnO nanowires. *Nanotechnology*, Vol. 18(20), 2007, p. 205503, ISSN: 1361-6528.

[16] Hsu, C. L.; Chang, S. J.; Hung, H. C.; Lin, Y. R.; Huang, C. J.; Tseng, Y. K.; Chen, I. C. (2005). Well-aligned, vertically Al-doped ZnO nanowires synthesized on ZnO:Ga/

Glass templates. *Journal of the Electrochemical Society*, Vol. 152(5), 2005, pp. G378-G381, ISSN: 0013-4651.

[17] Huang, M. H.; Wu, Y. Y.; Feick, H.; Tran, N.; Weber, E.; Yang, P. D. (2001). Catalytic growth of znic oxide nanowires by vapor transport. *Advanced Materials*, Vol. 13(2), Jan. 2001, pp. 113-116, ISSN: 1521-4095.

[18] Huang, Z. M.; Zhang, Y. Z.; Kotaki, M.; Ramakrishna, S. (2003). A review on polymer nanofibers by electrospinning and their applications in nanocomposites. *Compos. Sci. Technol.* Vol. 63, 2003; pp. 2223-2253, ISSN: 0266-3538.

[19] Huang, Y. H.; Bai, X. D.; Zhang, Y. (2006). In situ mechanical properties of individual ZnO nanowires and the mass measurement of nanoparticles. *J. Phys.: Condens. Matter*, Vol. 18, Mar. 2006, p. L179, ISSN: 1361-648X.

[20] Jeong, J. S.; Lee, J. Y. (2010). Substrate-facilitated nanoparticles sintering and component interconnection procedure. *Nanotechnology*, Vol. 21(47), Oct. 2010, p. 475204, ISSN: 1361-6528.

[21] Jiang, L.; Zhao, Y.; Zhai, J. (2004). A lotus-leaf-like superhydrophobic surface: a porous microsphere/nanofiber composite film prepared by electrohydrodynamics. *Angew. Chem. Int. Ed.*, Vol. 43, 2004, pp. 4338-4341, ISSN: 1521-3773.

[22] Kim, I. D.; Rothschild, A.; Lee, B. H.; Kim, D. Y.; Jo, S. M.; Tuller, H. L. (2006). Ultrasensitive chemiresistors based on electrospun TiO_2 nanofibers. *Nano. Lett.*, Vol. 6(9), 2006, pp. 2009-2013, ISSN: 1530-6984.

[23] Ko, S. H.; Lee, D.; Kang, H. W.; Nam, K. H.; Yeo, J. Y.; Hong, S. J.; Grigoropoulos, C. P.; Sung, H. J. (2011). Nanoforest of hydrothermally grown hierarchical ZnO nanowires for a high efficiency dye-sensitized solar cells. *Nano Letters*, Vol. 11(2), Jan. 2011, pp. 666-671, ISSN: 1530-6984.

[24] Kong, Y. C.; Yu, D. P.; Zhang, B.; Fang, W.; Feng, S. Q. (2001). Ultraviolet-emitting ZnO nanowires synthesized by a physical vapor deposition approach. *Appl. Phys. Lett.*, Vol. 78, Nov. 2001, p. 407, ISSN: 1616-3028.

[25] Kong, X. H.; Li, Y. D. (2003). Temperature-dependent regulation of antisense activity using a DNA/poly(N-isopropylacrylamide) conjugate. *Chemistry Letters*, Vol. 32(11), 2003, pp. 1062-1063, ISSN: 1348-0715.

[26] Kusinski, G. J.; Jokisaari, J. R.; Noriega, R.; Goris, L.; Donovan, M.; Salleo, A. (2010). Transmission electron microscopy of solution-processe, intrinsic and Al-doped ZnO nanowires for transparent electrode fabrication. *Journal of microscopy*, Vol. 237(3), Mar. 2010, pp. 443-449, ISSN: 1365-2818.

[27] Krishnakumar, T.; Jayaprakash, R.; Pinna, N.; Donato, N.; Bonavita, A.; Micali, G.; Neri, G. (2009). CO gas sensing of ZnO nanostructures synthesized by an assisted microwave wet chemical route. *Sensor and Actuators B: Chemical*, Vol. 143(1), Dec. 2009, pp. 198–204, ISSN: 092-4005.

[28] Landau, O.; Rothschild, A.; Zussman, E. (2009). Processing-microstructure-properties correlation of ultrasensitive gas sensors produced by electrospinning. *Chem. Mater.*, Vol. 21(1), Jan. 2009, pp. 9-11, ISSN: 0897-4756.

[29] Lee, W.; Jeong, M. C.; Myoung, J. M. (2004). Fabrication and application potential of ZnO nanowires grown on GaAs(002) substrates by metal-organic chemical vapour deposition. *Nanotechnol.*, Vol. 15(3), 2004, pp. 254-259, ISSN: 0957-4484.

[30] Li, M. M.; Long, Y. Z.; Tan, J. S.; Yin, H. X.; Sui, W. M.; Zhang, Z. (2010). Dielectric properties of electrospun titanium compound/polymer composite nanofibers. *Chin. Phys. B*, Vol. 19(2), Feb. 2010, p. 028102, ISSN: 1674-1056.

[31] Li, M. M.; Long, Y. Z.; Yang, D. Y.; Sun, J. S.; Yin, H.; Zhao, Z.; Kong, W.; Jiang, X.; Fan, Z. (2011). Fabrication of one dimensional superfine polymer fibers by double-spinning. *J. Mater. Chem.*, Vol. 21(35), 2011, pp. 13159-13162, ISSN: 1364-5501.

[32] Li, Y. J.; Li, K. M.; Wang, C. Y.; Kuo, C. I.; Chen, L. J. (2012). Low-temperature electrodeposited Co-doped ZnO nanorods with enhanced ethanol and CO sensing properties. *Sensor and Actuators B: Chemical*, Vol. 161(1), Jan. 2012, pp. 734-739, ISSN: 092-4005.

[33] Lin, D.; Wu, H.; Pan, W. (2007). Photoswitches and memories assembled by electrospinning aluminum doped zinc oxide single nanowires. *Advanced Materials*, Vol. 19(22), Oct. 2007, pp. 3968-3972, ISSN: 1521-4095.

[34] Liu, J. Z.; Lee, S.; Lee, K.; Ahn, Y. H.; Park, J. Y.; Koh, K. H. (2008). Bending and bundling of metal-free vertically aligned ZnO nanowires due to electrostatic interaction. *Nanotechnology*, Vol. 19(18), April 2008, p. 185607, ISSN: 1361-6528.

[35] Liu, L.; Zhang, T.; Wang, L. Y.; Li, S. C. (2009). Improved ethanol sensing properties of Cu-doped SnO_2 nanofibers. *Mater. Lett.* Vol. 63, Sep. 2009; pp. 2041-2043, ISSN: 0167-577X.

[36] Liu, C. Y.; Xu, H. Y.; Ma, J. G.; Li, X. H.; Zhang, X. T.; Liu, Y. C.; Mu, R. (2011). Electrically pumped near-ultraviolet lasing from ZnO/MgO core/shell nanowires. *Applied Physics Letters*, Vol. 99(6), 2011, p. 63115, ISSN: 1616-3028.

[37] Long, Y. Z.; Li, M. M.; Gu, C. Z.; Wan, M. X.; Duvail, J. L.; Liu, Z. W.; Fan, Z. Y. (2011). Recent advances in synthesis, physical properties and applications of conducting polymer nanotubes and nanofibers. *Progress in Polymer Science*, Vol. 36(10), Oct. 2011, pp. 1415-1442, ISSN: 0079-6700.

[38] Long, Y. Z.; Yu, M.; Sun, B.; Gu, C. Z.; Fan, Z. Y. (2012). Recent advances in large-scale assembly of semiconducting inorganic nanowires and nanofibers for electronics, sensors and photovoltaics. *Chem. Soc. Rev.*, Vol. 41(12), June 2012, pp. 4560-4580, ISSN: 0306-0012.

[39] Lü, H. F.; Xu, X. L.; Lü, L.; Gong, M. G.; Liu, Y. S. (2008). Photoluminescence enhancement of ZnO microrods coated with Ag nanoparticles. *J. Phys.: Condens. Matter*, Vol. 20(47), Dec. 2008, p. 472202, ISSN: 0953-8984.

[40] Nishino, T.; Meguro, M.; Nakamae, K.; Matsushita, M.; Ueda, Y. (1999). The lowest surface free energy based on $–CF_3$ alignment. *Langmuir*, Vol. 15(13), May 1999, p. 4321, ISSN: 1520-5827.

[41] Pan, Z. W.; Dai, Z. R.; Wang, Z. L. (2001). Nanobelts of semiconducting oxides. *Science*, Vol. 291, Feb. 2001; pp. 1947–1949, ISSN: 0036-8075.

[42] Pfüller, C.; Brandt, O.; Flissikowski, T.; Grahn, H. T.; Ive, T.; Speck, J. S.; DenBaars, S. P. (2011). Comparison of the spectral and temporal emission characteristics of homo-epitaxial and hetero-epitaxial ZnO nanowires. *Applied Physics Letters*, Vol. 98(11), Mar. 2011, p. 113113, ISSN: 1616-3028.

[43] Ra, Y.-W.; Choi, K.-S.; Kim, J.-H.; Hahn, Y.-B.; Im, Y.-H. (2008). Fabrication of ZnO nanowires using nanoscale spacer lithography for gas sensor. *Small*, Vol. 4(8), 2008, pp. 1105-1109, ISSN: 1613-6829.

[44] Richard, D.; Clanet, C.; Quere, D. (2002). Surface phenomena: contact time of a bouncing drop. *Nature*, Vol. 417, June 2002, p. 811, ISSN: 1061-4036.

[45] Sen, B.; Stroscio, M.; Dutta, M. (2011). Photoluminescence and Raman spectroscopy of polycrystalline ZnO nanofibers deposited by electrospinning. *Journal of Electronic Materials*, Vol. 40(9), 2011, pp. 2015-2019, ISSN: 0361-5235.

[46] Shan, W.; Walukiewicz, W.; Ager, J. W.; Yu, K. M.; Yuan, H. B.; Xin, H. P.; Cantwell, G.; Song, J. J. (2005). Nature of room-temperature photoluminescene in ZnO. *Appl. Phys. Lett.*, Vol. 86(19), May 2005, p. 191911, ISSN: 1616-3028.

[47] Shen, Y.; Hong, J.-I.; Xu, S.; Lin, S. S.; Fang, H.; Zhang, S.; Ding, Y.; Snyder, R. L.; Wang, Z. L. (2010). A general approach for fabricating arc-shaped composite nanowire arrays by pulsed laser deposition. *Advanced Functional Materials*, Vol. 20(5), Mar. 2010, pp. 703-707, ISSN: 1616-3028.

[48] Song, J. H.; Wang, X. D.; Riedo, E.; Wang, Z. L. (2005). Elastic property of vertically aligned nanowires. *Nano Lett.*, Vol. 5(10), Sep. 2005, pp. 1954-1958, ISSN: 1616-3028.

[49] Sui, X. M.; Shao, C. L.; Liu, Y. C. (2005). White-light emission of polyvinyl alcohol/ZnO hybrid nanofibers prepared by electrospinning. *Applied Physics Letters*, Vol. 87(11), 2005, pp. 113-115, ISSN: 1616-3028.

[50] Sun, B.; Long, Y. Z.; Yu, F.; Li, M. M.; Zhang, H. D.; Li, W. J.; Xu, T. X. (2012). Self-assembly of a three-dimensional fibrous polymer sponge by electrospinning. *Nanoscale*, Vol. 4(6), 2012, pp. 2134-2137, ISSN: 2040-3364.

[51] Tan, J. S.; Long, Y. Z.; Li, M. M. (2008). Preparation of aligned polymer micro/nanofibers by electrospinning. Chin. Phys. Lett., Vol. 25(8), Aug. 2008, pp. 3067-3070, ISSN: 0256-307X.

[52] Vayssieres, L.; Keis, K.; Lindquist, S. E.; Hagfeldt, A. (2001). Purpose-Built anisotropic metal oxide material: 3D highly oriented microrod array of ZnO. *Journal of Physical Chemistry B*, Vol. 105(17), Mar. 2001, pp. 3350-3352, ISSN: 1520-6106.

[53] Wang, X. D.; Summers, C. J.; Wang, Z. L. (2004). Large-scale hexagonal-patterned growth of aligned ZnO nanorods for nano-optoelectronics and nanosensor arrays. *Nano Letters*, Vol. 4(3), Jan. 2004, pp. 423-426, ISSN: 1530-6984.

[54] Wang, L. S.; Zhang, X. Z.; Zhao, S. Q.; Zhou, G. Y.; Zhou, Y. L.; Qi, J. J. (2005). Synthesis of well-aligned ZnO nanowire by simple physical vapor deposition on *c*-oriented ZnO thin films without catalysts or additives. *Applied Physics Letters*, Vol. 86(2), 2005, p. 024108, ISSN: 1616-3028.

[55] Wang, J. X.; Sun, X. W.; Yang, Y.; Huang, H.; Lee, Y. C.; Tan, O. K.; Vayssieres, L. (2006). Hydrothermally grown oriented ZnO nanorod arrays for gas sensing applications. *Nanotechnology*, Vol. 17(19), Sept. 2006, pp. 4995-4998, ISSN: 1361-6528.

[56] Wang, F. F.; Cao, L.; Pan, A. L.; Liu, R. B.; Wang, X.; Zhu, X.; Wang, S. Q.; Zou, B. S. (2007). Synthesis of tower-like ZnO structures and visible photoluminescence origins of varied shaped ZnO nanostructures. *J. Phys. Chem. C*, Vol. 111, 2007, p. 7655, ISSN: 1932-7447.

[57] Wang, Y.; Xu, X. L.; Xie, W. Y.; Wang, Z. B.; Lu, L.; Zhao, Y. L. (2008). Two-step growth of highly oriented ZnO nanorod arrays. *Acta Physica Sinica*, Vol. 57(4), Apr. 2008, pp. 2582-2586, ISSN: 1000-3290.

[58] Wang, J. X.; Sun, X. W.; Yang, Y.; Kyaw, K. K. A.; Huang, X. Y.; Yin, J. Z.; Wei, J.; Demir, H. V. (2011). Free-standing ZnO-CuO composite nanowier array films and their gas sensing properties. *Nanotechnology*, Vol. 22(32), July 2011, p. 325704, ISSN: 1361-6528.

[59] Wenzel, R. N. (1936). Resistance of solid surfaces to wetting by water. *Ind. Eng. Chem.*, Vol. 28(8), Aug. 1936, pp. 988-994, ISSN: 1226-086X.

[60] Wu, J. J.; Wen, H. I.; Tseng, C. H.; Liu, S. C. (2004). Well-aligned ZnO nanorods via hydrogen treatment of ZnO films. *Advanced Functional Materials*, Vol. 14(8), Sept. 2004, pp. 806-810, ISSN: 1616-3028.

[61] Wu, H.; Lin, D.; Zhang, R.; Pan, W. (2008). ZnO nanofiber field-effect transistor assembled by electrospinning. *Journal of the American Ceramic Society* 91 (2), Feb. 2008, 656-659, ISSN: 1551-2916.

[62] Xiao, X. H.; Ren, F.; Zhou, X. D.; Peng, T. C.; Wu, W.; Peng, X. N.; Yu, X. F.; Zhang, C. Z. (2010). Surface plasmon-enhanced light emission using silver nanoparticles embedded in ZnO. *Appl. Phys. Lett.*, Vol. 97, Aug. 2010, p. 071909, ISSN: 0003-6951.

[63] Xu, S.; Wang, Z. L. (2011). One-dimensional ZnO nanostructures: Solution growth and functional properties. *Nano Res.*, Vol. 4(11), 2011, pp. 1013-1098, ISSN: 1998-0124.

[64] Yang, J. L.; An, S. J.; Park, W. I.; Yi, G. C.; Choi, W. (2004). Photocatalysis using ZnO thin films and nanoneedles grown by metal-organic chemical vapor deposition. *Advanced Materials*, Vol. 16(18), Oct. 2004, pp. 1661-1664, ISSN: 1521-4095.

[65] You, J. B.; Zhang, X.W.; Fan, Y. M.; Qu, S.; Chen, N. F. (2007). Surface plasmon enhanced ultraviolet emission from ZnO films deposited on Ag/Si(001) by magnetron sputtering. *Appl. Phys. Lett.*, Vol. 91, Dec. 2007, p. 231907, ISSN: 1616-3028.

[66] Zeng, Y.; Zhang, T.; Wang, L. J.; Kang, M. H.; Fan, H.; Wang, R.; He, Y. (2009). Enhanced toluene sensing characteristics of TiO_2-doped flowerlike ZnO nanostructures. *Sensor and Actuators B*, Vol. 140, 2009, pp. 73–78, ISSN: 092-4005.

[67] Zhang, H. D.; Long, Y. Z.; Li, Z. J.; Sun, B.; Sheng, C. H. (2012). Synthesis, electrical and humidity sensing properties of BaTiO3 nanofibers via electrospinning. *Advanced Materials Research*, Vols. 418-420, 2012, pp. 684-687, ISSN: 1022-6680.

[68] Zheng, J.; Long, Y. Z.; Sun, B.; Zhang, Z. H.; Shao, F.; Zhang, H. D.; Zhang, Z. M.; Huang, J. Y. (2012). Polymer nanofibers prepared by low-voltage near-field electrospinning. *Chin. Phys. B*, Vol. 21(4), April 2012, p. 048102, ISSN: 1674-1056.

IntechOpen